

# Magnetostrictive behaviour of thin superconducting disks

Tom H. Johansen<sup>1,\*</sup> and Daniel V. Shantsev<sup>1,2</sup>

<sup>1</sup>*Department of Physics, University of Oslo, P. O. Box 1048 Blindern, 0316 Oslo, Norway*

<sup>2</sup>*A. F. Ioffe Physico-Technical Institute, Polytekhnicheskaya 26, St.Petersburg 194021, Russia*  
(March 22, 2022)

Flux-pinning-induced stress and strain distributions in a thin disk superconductor in a perpendicular magnetic field is analyzed. We calculate the body forces, solve the magneto-elastic problem and derive formulas for all stress and strain components, including the magnetostriction  $\Delta R/R$ . The flux and current density profiles in the disk are assumed to follow the Bean model. During a cycle of the applied field the maximum tensile stress is found to occur approximately midway between the maximum field and the remanent state. An effective relationship between this overall maximum stress and the peak field is found.

## I. INTRODUCTION

During recent years top-seeded growth of bulk Y-Ba<sub>2</sub>Cu<sub>3</sub>O<sub>y</sub> and (RE)-Ba<sub>2</sub>Cu<sub>3</sub>O<sub>y</sub> (RE = rare earth elements) has developed enormously towards production of large single-grain superconductors with strong flux pinning<sup>1,2</sup>. An impressive critical current density value of  $J_c = 100 \text{ kA/cm}^2$  at 77 K has now been obtained for bulk (Nd-Sm-Gd)-Ba<sub>2</sub>Cu<sub>3</sub>O<sub>y</sub> with 10 mol% of Gd-211.<sup>2</sup> Large-grain superconductors of this type can trap very high magnetic fields in the remanent state, exceeding the field from conventional permanent magnets by an order of magnitude and even more. Therefore, it is today strongly believed that the field-trapping ability of bulk superconductors is useful in many practical applications like magnetic separators, magnetron sputtering systems, motors etc.

A major problem of such bulks is that mechanical fracturing frequently occurs during the magnetic activation process. The strong flux pinning unavoidably leads to large body forces, which during descent of the applied field are tensile. Due to the irreversible nature of the flux dynamics, the resulting stress distribution becomes non-uniform, and can locally reach the tensile strength of the material so that fatal cracking takes place. A systematic study of this problem was first made by Ren et al.<sup>3</sup>, who also made model calculations of the internal stress in a cylindrical superconductor during the field descent after field-cooling. Later the modelling of the magneto-elastic behaviour has been extended considerably by including various geometrical cases and magnetization conditions<sup>4-9</sup>.

Common to all previous modelling work is that the superconductor is approximated as infinitely long in the direction of the applied field. Today, one sees that single-grain disks with diameters up to 6 cm are grown on routine basis,<sup>10</sup> whereas low-gravity environment has allowed growth of even larger disks - up to 12.7 cm in diameter and 2 cm in thickness.<sup>11</sup> When the diameter becomes much larger than the thickness the infinitely long cylinder approximation is known to give a poor description of flux and current distributions. A better approximation can then be a very thin sample in perpendicular field, where exact analytical results for flux distribution are also available. They were used to calculate magnetostriction for thin long strips in Ref. 14, but only for the virgin branch. In this work we use the thin disk solution, and find all the stresses and strains for the full magnetization cycle. We present here results of this model and discuss the relationship between the peak applied field and the overall maximum tensile stress occurring in the disk during pulsed field magnetic activation.

## II. MAGNETO-ELASTIC PROBLEM

Consider a thin superconducting circular disk of radius  $R$  and thickness  $d$ , where  $d \ll R$ . The superconductor is placed in a magnetic field,  $B_a$ , applied perpendicular to the disk plane, i.e., along the  $z$ -axis. When the local field at the edge exceeds the lower critical field,  $B_{c1}$ , the vortices start to penetrate into the disk. Due to strong demagnetization effects this happens already at  $B_a \geq \sqrt{d/R} B_{c1}$ . The presence of pinning centers will cause the vortices to distribute non-uniformly over the disk volume. According to the critical state model the quasi-stationary flux distribution adjusts irreversibly so that the local current density never exceeds the critical magnitude  $J_c$ . In analyses of this behaviour a common simplification is to ignore the effects of a lower critical field, and also the presence of any reversible magnetization. Under these conditions analytical results for the field and current distributions have been derived for the thin disk geometry.<sup>12</sup>

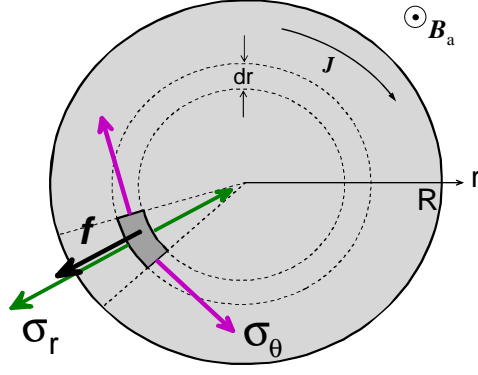


FIG. 1. Internal stresses and body forces in a superconducting disk placed in a perpendicular applied magnetic field.

The force per unit volume acting on the vortices is given by the Lorentz force  $\mathbf{f} = \mathbf{J} \times \mathbf{B}$ , where  $\mathbf{J}$  and  $\mathbf{B}$  are the local current and flux density, respectively. In quasi-static equilibrium this force is balanced by pinning forces, and hence,  $\mathbf{f}$  also represents the distribution of body forces transmitted onto the crystal lattice in a given magnetized state. The symmetry of the disk geometry implies that the induced current has only an azimuthal component, and the force averaged over the disk thickness points in the radial direction, see Fig. 1.

For the thin disk one can therefore write

$$f(r) = J(r)B(r), \quad (1)$$

where  $J(r)$  is the current density averaged over  $d$ , and  $B(r) \equiv B_z(z=0)$  is the flux density in the disk's center plane.

Exact analytical results for a thin disk in perpendicular field are available only for the Bean model, where  $J_c$  is assumed field-independent. We adopt this model in the present analysis, and review here only the results needed for the calculations of the magneto-elastic behavior.

Starting with a flux free superconductor the application of a magnetic field,  $B_a$ , will cause penetration of flux into the disk up to the point  $r = a$ , where

$$a = \frac{R}{\cosh(B_a/B_d)} \quad \text{and} \quad B_d = \mu_0 J_c d/2. \quad (2)$$

In the annular vortex-filled region the flux density has the strongly non-linear profile given by

$$\frac{B(r)}{B_d} = \frac{B_a}{B_d} - \text{arccosh}(R/r) + \frac{2}{\pi} \int_{\arcsin(a/r)}^{\pi/2} \frac{1 - \theta \cot \theta}{\sqrt{1 - (r/R)^2 \sin^2 \theta}} d\theta, \quad a \leq r \leq R. \quad (3)$$

The central region  $r \leq a$  has  $B = 0$ , as for the long cylinder.

The shielding current is for a thin disk distributed over the entire area according to

$$J(r)/J_c = \begin{cases} -1, & a \leq r < R, \\ -\frac{2}{\pi} \arctan \left( \frac{r}{R} \sqrt{\frac{R^2 - a^2}{a^2 - r^2}} \right), & r \leq a. \end{cases} \quad (4)$$

Note here that  $J$  is *not* proportional to the flux density gradient  $dB/dr$ , thus preventing us from using the relation  $f dr = -d(B^2)/2\mu_0$ , which is valid for a long cylinder. Figure 2 (top) shows graphs of the body force distribution, Eq.(1), during virgin magnetization of the disk. Since the current has a constant magnitude where the flux density is non-zero, the force profile has the same shape as the function  $B(r)$ .

When the applied field is reduced after reaching a maximum value  $B_a^{\max}$ , the disk undergoes remagnetization where the front is located at  $r = b$ , with

$$b = \frac{R}{\cosh [(B_a^{\max} - B_a)/2B_d]}. \quad (5)$$

In the inner region,  $r < b$ , the flux density generated by the maximum field is unchanged, whereas in the outer annulus,  $b \leq r < R$ , considerable redistribution of flux is taking place. The current, on the other hand, becomes

modified in the entire disk area. During field reduction the disk is therefore divided into three regions, each described by its own set of functions  $J(r)$ ,  $B(r)$  and thereby also  $f(r)$ . One has for:

Region I (outer);  $b \leq r < R$ ;

$$\frac{B(r)}{B_d} = \frac{B_a}{B_d} + \operatorname{arccosh}(R/r) + \frac{2}{\pi} \left[ \int_{\arcsin(\hat{a}/r)}^{\arcsin(b/r)} \frac{1 - \theta \cot \theta}{\sqrt{1 - (r/R)^2 \sin^2 \theta}} d\theta - \int_{\arcsin(b/r)}^{\pi/2} \frac{1 - \theta \cot \theta}{\sqrt{1 - (r/R)^2 \sin^2 \theta}} d\theta \right],$$

$$J(r)/J_c = 1. \quad (6)$$

Region II (middle);  $\hat{a} \leq r < b$ ;

$$\frac{B(r)}{B_d} = \frac{B_a^{\max}}{B_d} - \operatorname{arccosh}(R/r) + \frac{2}{\pi} \int_{\arcsin(\hat{a}/r)}^{\pi/2} \frac{1 - \theta \cot \theta}{\sqrt{1 - (r/R)^2 \sin^2 \theta}} d\theta,$$

$$\frac{J(r)}{J_c} = -1 + \frac{4}{\pi} \arctan \left( \frac{r}{R} \sqrt{\frac{R^2 - b^2}{b^2 - r^2}} \right) \quad (7)$$

Region III (inner);  $r < \hat{a}$ ;

$$\frac{J(r)}{J_c} = \frac{2}{\pi} \left[ 2 \arctan \left( \frac{r}{R} \sqrt{\frac{R^2 - b^2}{b^2 - r^2}} \right) - \arctan \left( \frac{r}{R} \sqrt{\frac{R^2 - \hat{a}^2}{\hat{a}^2 - r^2}} \right) \right]$$

$$B(r) = 0, \quad (8)$$

Shown in Fig. 2 (bottom) are plots of  $f(r)$  at various stages of field reduction. A cusped peak in the body force is seen to accompany the remagnetization front at  $r = b$ . After reversing the field sweep the outer part of the disk immediately starts to experience forces that will create tension. When the field has been reduced to zero considerable remanent body forces, a mixture of tensile and compressive forces, remain in the disk.

To determine the quantitative magnetostrictive behaviour a separate analysis of the thin disk elasticity problem is required. For simplicity, we assume that the superconductor is mechanically isotropic, and that the strains are well below the fracture limit allowing linear elasticity theory to be applicable. As mechanical boundary conditions for the disk we choose a free surface, i.e., the normal stresses,  $\sigma_r$  and  $\sigma_z$  vanish at the surfaces. Moreover, since the disk is thin one can assume that  $\sigma_z = 0$  throughout the volume, and that the deformation is described by only a radial displacement field,  $u(r)$ . The strain components are then

$$e_r = u'(r) \quad \text{and} \quad e_\theta = u/r, \quad (9)$$

which are related to the non-vanishing stresses  $\sigma_r$  and  $\sigma_\theta$  by

$$Ee_r = \sigma_r - \nu\sigma_\theta \quad \text{and} \quad Ee_\theta = \sigma_\theta - \nu\sigma_r. \quad (10)$$

Here  $E$  and  $\nu$  is the Young's modulus and Poisson's ratio, respectively. The condition of static equilibrium, see Fig. 1, is that

$$\sigma_r'(r) + \frac{\sigma_r - \sigma_\theta}{r} + f = 0, \quad (11)$$

which in terms of the displacement field is expressed as

$$u'' + \frac{1}{r}u' - \frac{1}{r^2}u + \frac{1 - \nu^2}{E}f = 0, \quad (12)$$

or

$$\frac{d}{dr} \left[ \frac{1}{r} \frac{d(ur)}{dr} \right] = -\frac{1 - \nu^2}{E}f. \quad (13)$$

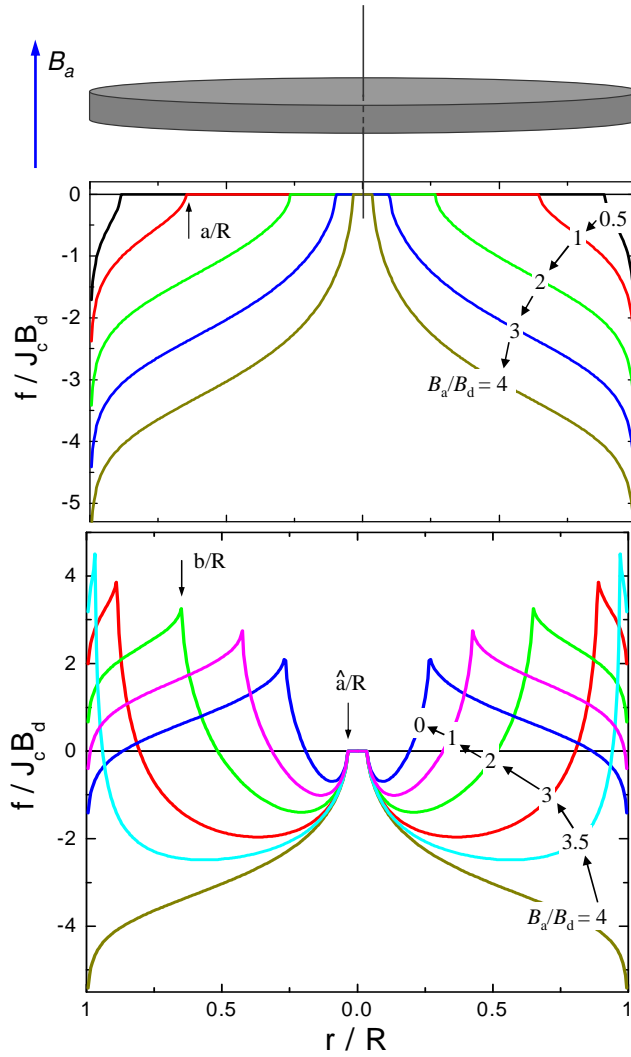


FIG. 2. Body force distribution in a disk during field rise from the virgin state (top), and subsequent field descent (bottom). Positive force means that it points radially *out* from the center.

Integrating twice, and using that  $\sigma_r(r = R) = 0$ , and  $u(0) = 0$ , one obtains

$$u(r) = \frac{1-\nu}{2E} r \left[ \left( \frac{1-\nu}{R^2} + \frac{1+\nu}{r^2} \right) \int_0^r r'^2 f dr' + \int_r^R \left( 1+\nu + \frac{1-\nu}{R^2} r'^2 \right) f dr' \right]. \quad (14)$$

It immediately follows that the external dilatation  $\Delta R = u(R)$  is given by

$$\frac{\Delta R}{R} = \frac{1-\nu}{E} \frac{1}{R^2} \int_0^R r'^2 f dr'. \quad (15)$$

The internal strains can be expressed as

$$\begin{aligned} e_r(r) &= \frac{1-\nu}{2E} \left[ \left( \frac{1-\nu}{R^2} \mp \frac{1+\nu}{r^2} \right) \int_0^r r'^2 f dr' + \int_r^R \left( 1+\nu + \frac{1-\nu}{R^2} r'^2 \right) f dr' \right], \\ e_\theta(r) &= \frac{1-\nu}{2E} \left[ \left( \frac{1-\nu}{R^2} \mp \frac{1+\nu}{r^2} \right) \int_0^r r'^2 f dr' + \int_r^R \left( 1+\nu + \frac{1-\nu}{R^2} r'^2 \right) f dr' \right], \end{aligned} \quad (16)$$

with the upper and lower sign corresponding to  $e_r$  and  $e_\theta$ , respectively. Similarly, the radial stress and the hoop stress are given by

$$\begin{aligned} \sigma_r(r) &= \frac{1-\nu}{2} \left[ \left( \frac{1}{R^2} \mp \frac{1}{r^2} \right) \int_0^r r'^2 f dr' + \int_r^R \left( \frac{1+\nu}{1-\nu} + \frac{r'^2}{R^2} \right) f dr' \right], \\ \sigma_\theta(r) &= \frac{1-\nu}{2} \left[ \left( \frac{1}{R^2} \mp \frac{1}{r^2} \right) \int_0^r r'^2 f dr' + \int_r^R \left( \frac{1+\nu}{1-\nu} + \frac{r'^2}{R^2} \right) f dr' \right]. \end{aligned} \quad (17)$$

The eqs.(14-17) are exact expressions from which the magneto-elastic response can be calculated once the force distribution  $f(r)$  is known. One can see immediately that the two strains and the two stresses are equal in the center, i.e.,  $e_r(0) = e_\theta(0)$  and  $\sigma_r(0) = \sigma_\theta(0)$ , independent of the magnetized state. Notice also that the hoop stress at the rim of the disk is proportional to the dilatation,  $\sigma_\theta(R) = E\Delta R/R$ , as it should according to Eq. (10) and the condition  $\sigma_r(R) = 0$ .

### III. RESULTS AND DISCUSSION

#### A. Magnetostriction $\Delta R/R$

The irreversible behaviour of the magnetostriction,  $\Delta R/R$ , as a function of the applied field,  $B_a$ , is calculated from Eq. (15) using the expressions for  $J(r)$  and  $B(r)$  that were listed in the previous section. The result is shown in Fig. 3 (left), where hysteresis loops with three different maximum fields are plotted. The overall shape of the loops is quite similar to that found in the long cylinder case.<sup>6</sup> When the maximum applied field becomes much higher than  $B_d$  a large part of the loop is well represented by two straight lines forming a cross centered at  $B_a = 0$ . Asymptotically, this linear behaviour is described by

$$\frac{\Delta R}{R} = \frac{1-\nu}{E} J_c R B_d \left( \pm \frac{B_a}{3B_d} + 7.57 \cdot 10^{-2} \right). \quad (18)$$

Therefore, the width of large field ( $B_a^{\max} \gg B_d$ ) hysteresis loop rapidly approaches

$$(\Delta R/R)_\downarrow - (\Delta R/R)_\uparrow = 2 \frac{1-\nu}{E} J_c R B_a. \quad (19)$$

Interestingly, the same simple relation holds also for the long cylinder when  $B_a^{\max} > 2B_p$ , where  $B_p = \mu_0 J_c R$  is the full penetration field.<sup>6</sup> The virgin branches of the loops are not included in Fig. 3 since on the chosen scale they are barely resolved.

The corresponding result for thin long strips is given by Eqs. 16-17 of Ref. 14. For large  $B_a^{\max}$  it reduces to our Eq. (19), except that the factor  $1-\nu$  is missing. This factor should appear when the stress from the currents on the far edges of the strip is taken into account, as also discussed in Ref. 14.

Dilatation loops found experimentally<sup>13,14</sup> can deviate from the shown Fig. 3 (left) due to a field dependence of the critical current. If this dependence is rather strong, the loops will narrow down for large fields, as shown in Fig. 3 (right). These curves were calculated assuming an exponential dependence of the critical current,  $J_c(B) = J_c(0) \exp(-|B|/2B_d)$ . Flux and current distributions cannot be written down explicitly in case of field-dependent  $J_c$ , however they can be found numerically by solving a set of integral equations given in Ref. 15. It allows calculation of magnetization loops, as explained in Ref. 16, where  $M$  decreases with  $B$  at large fields in accordance with chosen  $J_c(B)$  dependence. A similar procedure was used to calculate the dilatation loops of Fig. 3 (right).

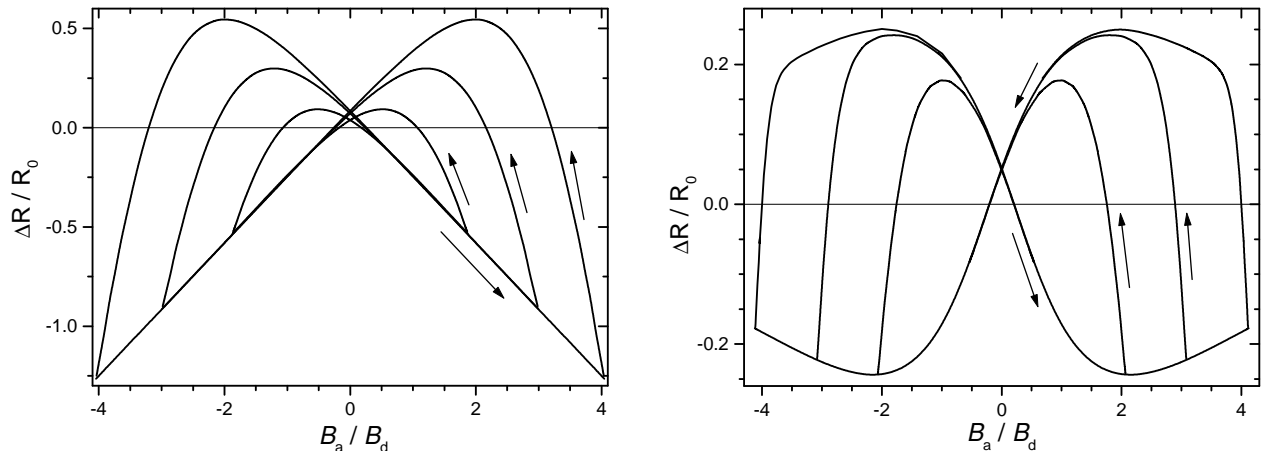


FIG. 3. Dilatation loops for cycles of  $B_a$  with a different maximum field. The dilatation is normalized by  $R_0 = (1-\nu)J_c B_d R/E$ . Left: the Bean model. Right: a field-dependent critical current,  $J_c(B) = J_c(0) \exp(-|B|/2B_d)$ .

## B. Stress Distributions

As the applied field increases, the body force points towards the disk centre, leading to stresses that everywhere are compressive (negative). During the ramp up of the field the compressive stress grows monotonically, and always with a spatial distribution where the central unpenetrated region experiences the largest compression. Since these stress values are normally much lower than the compressive strength of the superconductor, we focus here instead on the descending field stage of the magnetic activation process.

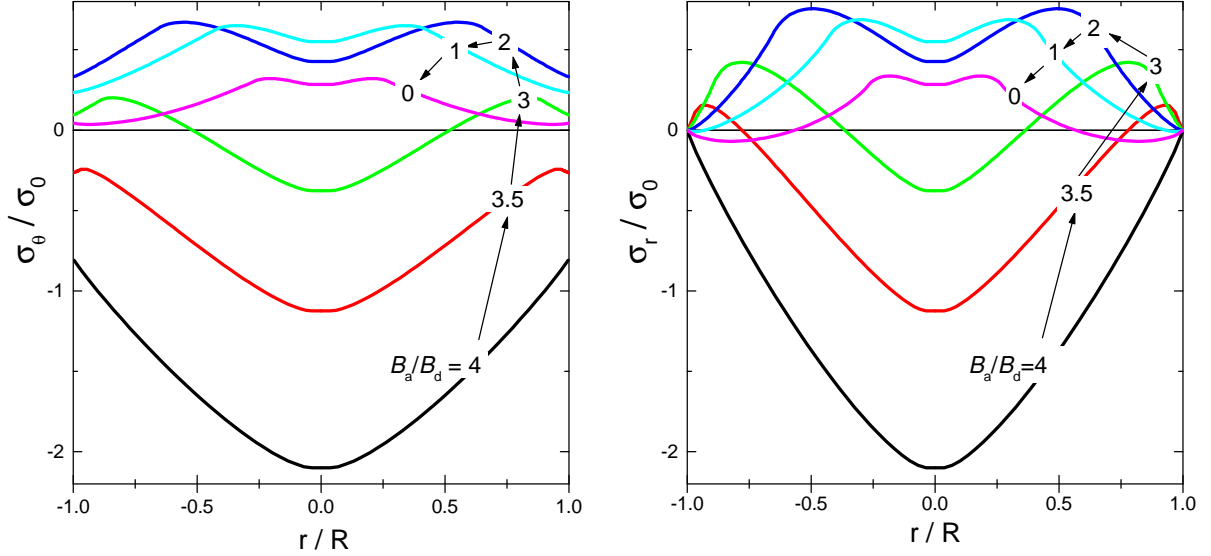


FIG. 4. Distribution of the hoop (left) and radial (right) stresses in a disk during the field decent after reaching a maximal value  $B_a = 4B_d$ . The stress is normalized by  $\sigma_0 \equiv B_d J_c R$  and  $\nu = 0.3$  was used in the calculations.

As an example, let us consider the case where the maximum applied field has the value  $B_a^{\max} = 4B_d$ . When  $B_a$  starts to decrease, the stress distribution becomes more complex since the body force turns expansive in the outer remagnetized region. The Fig. 4 illustrates how the stresses develop during the field descent. Very soon a peak of tensile (positive) stress appears near the remagnetization front, and the peak value grows in height. At an intermediate field the peak tension reaches an overall maximum, which for the radial stress amounts to  $0.8\sigma_0$ , where  $\sigma_0 = B_d J_c R$ . The maximum hoop stress is slightly smaller. It is during this part of the field descent the disk is most likely to crack, namely the first time the material encounters a stress equal to the tensile strength.

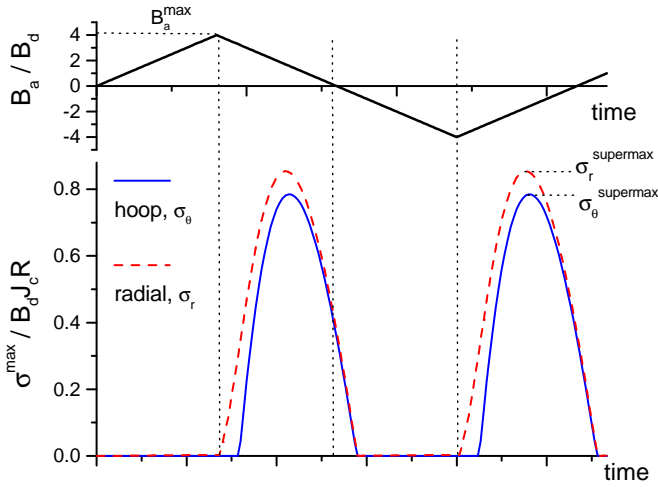


FIG. 5. Time evolution of maximal tensile stress in the disk during a full cycle of applied field starting from the virgin state.

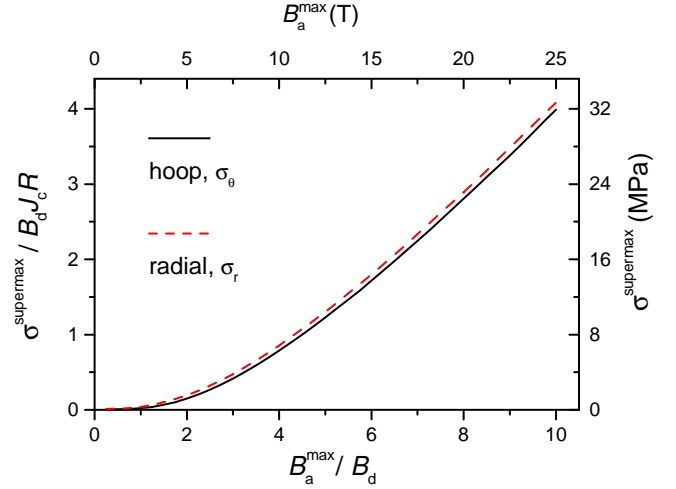


FIG. 6. The overall maximal stress reached during the full field cycle, as found from Fig. 5, versus the applied field amplitude. The dimensional values on the right and top axes are given for a typical disk with parameters given in the text.

Shown in Fig. 5 is the time evolution of the stresses during one full cycle of the applied field. The curves show the maximum tension occurring in the disk. The parts given zero value correspond to the stages where the stress is everywhere compressive. It becomes evident that the most 'dangerous' stage of the process is slightly after midway between the maximum field and the remanent state. The tension in the remanent state is roughly twice smaller than the overall maximum value, which we denote as  $\sigma^{\text{supermax}}$ . The next Figure shows how this  $\sigma^{\text{supermax}}$  depends on the maximum applied field in the cycle. The dependence is essentially parabolic, and is well fitted by a simple formula,

$$\frac{\sigma^{\text{supermax}}}{B_d J_c R} = 0.063 \frac{B_a^{\text{max}}}{B_d} + 0.035 \left( \frac{B_a^{\text{max}}}{B_d} \right)^2 \quad (20)$$

By substituting the following realistic numbers for disk parameters;  $J_c = 10 \text{ kA/cm}^2$ ,  $d = 2 \text{ cm}$ ,  $R = 3 \text{ cm}$ , one obtains dimensional values for the peak tension versus the maximal applied field as shown in the top and right axes of Fig. 6. This graph represents the essence of the present work, and may hopefully serve as a useful guide in practical situations. E.g. it follows that for a disk with tensile strength of 20 MPa,<sup>17</sup> one has to apply a field less than 18 T to avoid cracking during the pulsed-field activation.

The results presented here are obtained in the limit of thin disk in perpendicular field. Combined with the previous results for a long cylinder<sup>6</sup>, they give two extreme cases between which all real samples fall into. Unfortunately, the analytical treatment for samples with finite thickness is not possible, and numerical results are not available. Therefore, we may only hope that the key quantities, like magnetostriction and maximal tensile stress, show a smooth interpolation behavior between the two extreme cases. Additional reason for this hope is a very smooth interpolation behavior for magnetization and the penetration field that have already been calculated numerically for arbitrary thickness.<sup>18</sup> For example, the normalized  $M(H)$  curves for all thickness/radius ratios differ by not more than 3% from some average  $M(H)$ . It should be mentioned that our magnetostriction plots for long cylinder<sup>6</sup> and thin disk, Fig. 3, also show a remarkable similarity.

In conclusion, we solve the magneto-elastic problem and find stress, strain and magnetostriction in a thin disk superconductor for the full cycle of applied field. The maximum tensile stress occurs approximately midway between the maximum field and the remanent state, see Fig. 5, and has quasi-parabolic dependence on the peak field, see Eq. (20). Qualitative behavior of the stress and strain components, and the normalized magnetostriction loop is similar to the case of long cylinder.

### C. Acknowledgements

The work was financially supported by the Norwegian Research Council and NorFa.

\* Email for correspondence: t.h.johansen@fys.uio.no

- <sup>1</sup> M. Murakami, N. Sakai, T. Higuchi and S. I. Yoo, Supercond. Sci. Technol. **9** 1015 (1996).
- <sup>2</sup> M. Muralidhar, M. Jirsa, N. Sakai and M. Murakami, Supercond. Sci. Technol. **16** R1 (2003).
- <sup>3</sup> Y. Ren, R. Weinstein, J. Liu, R. P. Sawh and C. Foster, Physica C **251** 15 (1995).
- <sup>4</sup> T. H. Johansen, J. Lothe and H. Bratsberg. Phys. Rev. Lett. **80**, 4757 (1998).
- <sup>5</sup> T. H. Johansen, Phys. Rev. B **59** 11187 (1999).
- <sup>6</sup> T. H. Johansen, Phys. Rev. B **60** 9690 (1999).
- <sup>7</sup> T. H. Johansen, Supercond. Sci. Technol. **13** R121 (2000).
- <sup>8</sup> T. H. Johansen, C. Wang, Q. Y. Chen and W.-K. Chu, J. Appl. Phys. **88**, 2730 (2000).
- <sup>9</sup> T. H. Johansen, Q. Y. Chen and W.-K. Chu, Physica C **349**, 201 (2001).
- <sup>10</sup> U. Mizutani et al., report presented at the 2nd Workshop on Mechano-Electromagnetic Property of Composite Superconductors, Kyoto (2003).
- <sup>11</sup> M. Murakami et al., report presented at the 2nd Workshop on Mechano-Electromagnetic Property of Composite Superconductors, Kyoto (2003).
- <sup>12</sup> J. Clem and A. Sanchez, Phys. Rev. B **50** 9355 (1994).
- <sup>13</sup> H. Ikuta, N. Hirota, Y. Nakayama, K. Kishio and K. Kitazawa, Phys. Rev. Lett. **70** 2166 (1993).
- <sup>14</sup> N. Nabialek, H. Szymczak, V. A. Sirenko and A. I. D'yashenko, J. Appl. Phys. **84** 3770 (1998).
- <sup>15</sup> D. V. Shantsev, Y. M. Galperin and T. H. Johansen, Phys. Rev. B **60** 13112 (1999).
- <sup>16</sup> D. V. Shantsev, Y. M. Galperin and T. H. Johansen, Phys. Rev. B **61** 9699 (2000).
- <sup>17</sup> M. Tomita, M. Murakami and K. Yoneda, Supercond. Sci. Technol. **15** 803 (2002).
- <sup>18</sup> E. H. Brandt, Phys. Rev. B. **54** (1996) 4246.